

http://pubs.acs.org/journal/aesccq Article

Paleoenvironmental Reconstruction and Organic Matter Accumulation of the Lower Cambrian Qiongzhusi Formation in the Sichuan Basin, South China

Leibo Bian,* Niels H. Schovsbo, Anthony Chappaz, Arka Rudra, Jin Xu, Qingyong Luo, and Hamed Sanei*



Cite This: ACS Earth Space Chem. 2022, 6, 2519-2529



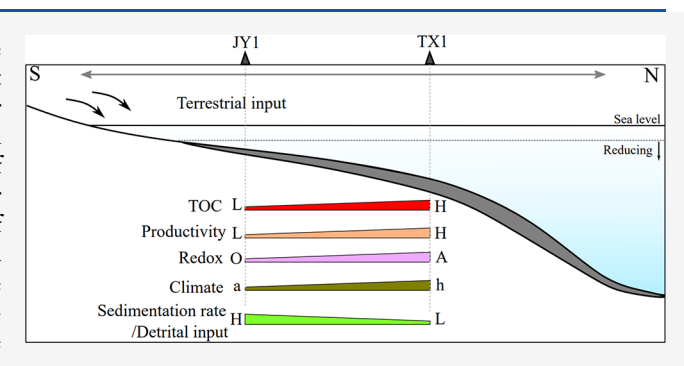
ACCESS

III Metrics & More

Article Recommendations

3 Supporting Information

ABSTRACT: The lower Cambrian Qiongzhusi Formation in the Sichuan Basin of the Yangtze Platform is one of the most proliferous petroleum sources. However, the basin-wide lower Cambrian (Qiongzhusi) environmental variation in the Sichuan Basin remains unclear, which could have impeded the unlocking of promising areas of organic matter accumulation. This paper presents the first detailed inorganic geochemical investigation of the lower Cambrian environmental reconstruction in the Sichuan Basin. The results of principal component analysis show that the lower Qiongzhusi succession (LQS) is enriched in carbonate-associated elements and rare earth elements (REE), whereas the middle—upper Qiongzhusi successions (MQS—UQS) are enriched



in elements affiliated with aluminosilicates (e.g., Al and Ti). The conservative metal associations suggest that the provenance of the sediments was intermediate-felsic igneous rocks and the tectonic setting was a continental island arc. The combination of Sr/Ba and S/TOC values indicates that it was formed under brackish to normal marine conditions. In contrast to the middle Qiongzhusi succession, the lower and upper Qiongzhusi successions had elevated biological productivity (increased Cu/Al), low detrital inputs (decreased Ti/Al), low sedimentation rate (decreased Th/U), and reducing conditions. These attributes probably resulted in higher organic matter productivity and preservation. Temporally, the northern part of this basin had higher organic matter contents and was deposited under more reducing conditions, with a lower sedimentation rate of terrigenous materials.

KEYWORDS: elemental composition, paleoenvironmental dynamics, organic matter preservation, Sichuan Basin, Qiongzhusi formation, lower Cambrian

1. INTRODUCTION

The reconstruction of the paleoenvironment is crucial because it can affect organic matter productivity and preservation, which further influence the distribution and reserve of hydrocarbon resources. Paleoenvironmental indicators, such as the paleoclimate, water circulation and salinity, and redox conditions, are preserved and recorded through elemental abundances and mineral compositions. Therefore, the elemental and mineral assemblages are widely considered as effective and crucial approaches for reconstructing the paleodepositional environment.

The lower Cambrian (Qiongzhusi) source rock is one of the proliferous source rocks in the Sichuan Basin of the Yangtze Platform, which have contributed to significant hydrocarbon resources. 9–11 Organic matter productivity and preservation in organic-rich rocks are generally influenced by the paleoenvironment. Previous studies have investigated the environmental variation in the central Sichuan Basin. 10,11 However, the absence of a basin-scale geochemical investigation contrasting

the depositional environment may have influenced the evaluation of lower Cambrian hydrocarbon resources in the Sichuan Basin. In addition, since the Qiongzhusi samples have high thermal maturity (1.2 to 4.4% of vitrinite-equivalent reflectance¹²) and a high degree of thermal degradation of organic matter, ^{13–15} conventional organic geochemical methods may not be used to reconstruct the depositional environment of this basin. Our objectives were to (i) use inorganic geochemical proxies to reconstruct the lower Cambrian environment and (ii) infer the potential areas for high organic matter productivity and preservation within the Sichuan Basin.

Received: July 25, 2022 Revised: August 24, 2022 Accepted: September 2, 2022 Published: September 14, 2022





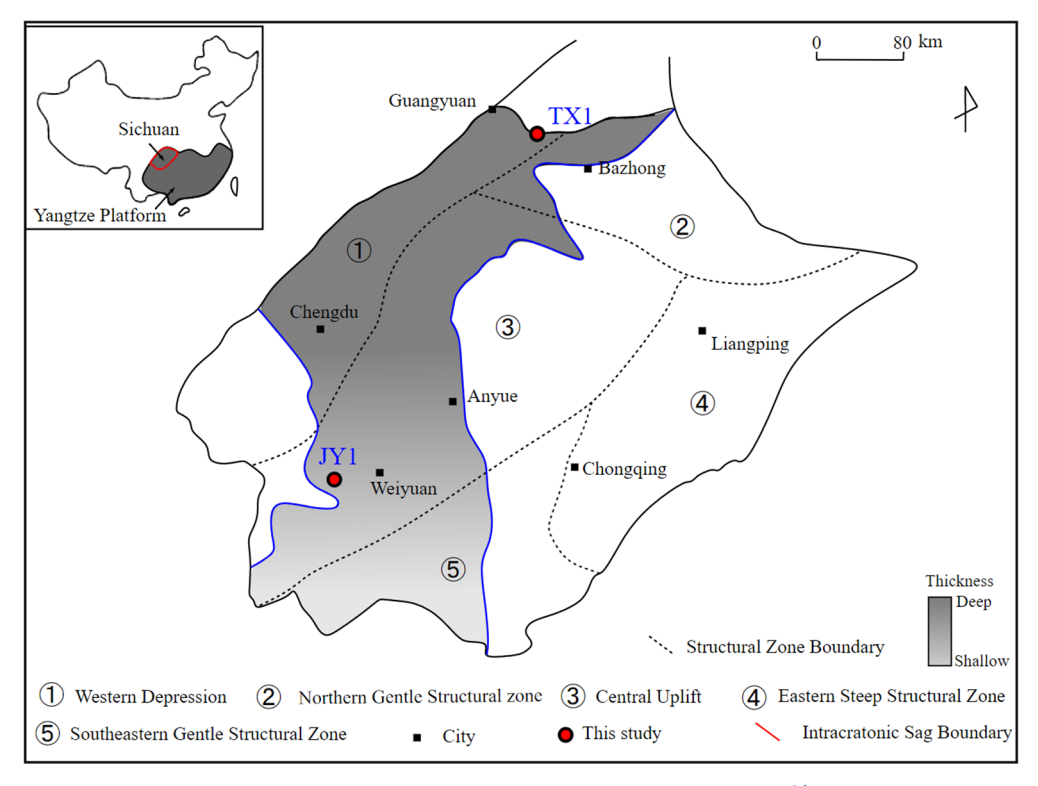


Figure 1. Location of the studied cores in the Sichuan Basin, South China. Modified from Liu et al. 16

2. GEOLOGICAL SETTING AND STUDIED CORES

The Sichuan Basin covers an area of more than 180,000 km² and is located in the northwestern part of the Yangtze Platform (Figure 1). During the early Cambrian, the Yangtze Platform was at the Northern Hemisphere latitude and was likely close to Australia in eastern Gondwana, based on a comparison of bioprovinces. 17 Previous studies suggested that the Sichuan Basin was a rather shallow water basin. 18 Within the Sichuan Basin, the lower Cambrian strata were deposited from the Terreneuvian to early Series 2 (Fortunian - Stage 3), 19,20 chronostratigraphically corresponding to the Niutitang Formation of the Yangtze Platform. 20 The Qiongzhusi source rock was deposited in the Mianyang-Changning intracratonic sag of the Sichuan Basin. 10,16 This sag is an asymmetrical, striking intracratonic sag with a relatively gentle western slope and a rather steep eastern slope. 16 The middle part of this sag is relatively narrow and becomes wider toward the southern and northern parts (Figure 1). The JY1 core was drilled in the southwestern part of this basin, and the TX1 core was drilled in the northern part (Figure 1).

The JY1 core can be divided into three successions (Figure S1). Abundant small shelly fossils, radiolarians, spongy spicules, and cryptospores were identified in the lower Qiongzhusi succession. Two trilobite biozones, namely, the Tsunyidiscus acutus—yanjiazhaiensis and Eoredlichia—Wutingaspis biozones, and three bradoriida biozones, namely, Liangshanella—Tsunyiella, Emeiella—Kunmingella fusulus, and Kunmingella dowille—Chuandianella ovata—mononotella biozones, were recognized in the middle—upper Qiongzhusi. The lithology of the lower Qiongzhusi succession (LQS) is dark phosphatic, fine-crystal dolomites intercalated with siliceous phosphorite, mudstone, and siltstone. The middle Qiongzhusi succession (MQS) can be divided into two subsections in descending order, zone I and zone II. The

lithology of the MQS zone II changes upward from black mudstone to the interbedding of grayish mudstone and siltstone. The MQS zone I is mainly composed of mudstone intercalated with siltstone. In the upper Qiongzhusi succession (UQS), the lithology comprises mudstone and siltstone.

The TX1 core is divided into zones I and II of MQS (Figure S2). The lithology of the TX1 core is composed of mudstone and siltstone. Zone I is slightly enriched in clay minerals compared to zone II (Figure 4). The LQS and UQS are absent in the TX1 core. The UQS in the northern Sichuan Basin has not been reported to date. Xia et al.²² documented that the LQS source rock has high TOC contents (0.70–42.70 wt %) with an average value of 12.95 wt %, dominated by marine-type kerogen. The bitumen reflectance varies from 1.56 to 2.83%, suggesting that the rocks are mature to highly mature. The lithology is mudstone and phosphatic, fine-crystal dolomite, similar to the LQS of the JY1 core.

3. SAMPLES AND METHODS

A total of 108 samples were obtained from the JY1 and TX1 cores. In the JY1 core, 24 samples are from the lower Qiongzhusi succession, 29 samples are from the middle succession, and 15 samples are from the upper succession. Forty samples are collected in the TX1 core. All analytical experiments were conducted at the State Key Laboratory of Shale Oil and Gas Enrichment and Effective Development (Wuxi), and analytical results are provided in the Supplementary Material.

3.1. Analytical Methods. 3.1.1. Total Organic Carbon and Sulfur Analyses. Total organic carbon (TOC) and sulfur (S) contents were measured using a LECO CS200 analyzer. Around 50 mg of the powdered sample was treated with 2 M HCl to remove the carbonate parts and subsequently dried in an oven at below 100 °C for 12 h. After that, the dried sample

was heated at 900 °C for 5 min to measure the TOC and S contents. The analytical precision is better than 5%.

- 3.1.2. Elemental Analysis. Elements were determined by inductively coupled plasma mass spectrometry (VISTA MPX). Approximately 150 mg of the powdered sample was dissolved in a mixed HNO $_3$ (0.5 mL) and HF (1 mL) solution and subsequently kept in an oven at 185 \pm 5 °C for 24 h. After that, to the residue was added 0.5 mL of HNO $_3$, and the mixture was kept at 185 \pm 5 °C for 24 h. The final insoluble residue was digested with a 5 mL HNO $_3$ solution (30% v/v) at 130 °C for 3 h before being diluted to 50 mL by distilled water for analysis. Data accuracy and variability were checked by reference materials (GBW 07112, GBW 07114, and SGR1b), replicated samples (\pm 5% analytical precision), and blanks.
- 3.1.3. X-ray Diffractometry. Mineralogy was measured using the X-ray diffractometer (Bruker D8 Advance). Samples were pulverized into less than 74 μ m prior to analysis. Minerals were recognized by the diffraction pattern with Cu-filtered radiation and 2θ step scans of 0.02° scanning from 2 to 90° with a speed of $2^{\circ}/s$. The identification of minerals was made using the Rietveld method.²³ The detected mineral contents were normalized to 100%, and a semi-quantitative relative mineral abundance was provided.
- **3.2. Statistical Analysis.** The principal component analysis (PCA) method was used to identify the geochemical affinities among the LQS, MQS, and UQS. In brief, all data were first transformed into the same unit (ppm) before the center logarithm ratio (CLR) normalization that is typically used when compositional (closed) data is examined.²⁴ The calibrated dataset was analyzed using the PCA method with the indiscriminate pretreatment for sample clusters. The PCA method was conducted through the program Past 3.26b.²⁵ The detailed analytical procedures refer to Bian et al.²⁶

4. RESULTS

- **4.1. Mineralogy.** The minerals in the LQS are composed of quartz (median value: 33%, hereinafter), dolomite (15%), siderite (12%), pyrite (10%), clay minerals (7%), and barite (6%). In the MQS, the minerals in zone I are clay minerals (38%), quartz (34%), feldspar (14%), carbonate matrix (9%), and Fe minerals (3%). Similarly, quartz (40%) and clay minerals (33%) are the main minerals in zone II, followed by feldspar (13%), carbonate matrix (9%), and Fe minerals (3%). In the UQS, the median clay mineral content increases to 51%, followed by quartz (31%), feldspar (8%), carbonate matrix (5%), and Fe minerals (5%). In contrast to the JY1 core, the TX1 core is enriched in clay minerals and feldspar. The ternary diagram shows that carbonates, quartz, and feldspar (>90%) account for the major minerals in the LQS, whereas clay minerals, quartz, and feldspar (>90%) are the main part in the MQS-UQS (Figure 2).
- **4.2. Elemental Compositions.** *4.2.1. Elemental Associations.* The PCA method is used to differentiate elemental compositions of the UQS, MQS, and LQS. In our model, the first two PCs account for 80% of the variance (PC1: 67% and PC2: 13%) (Figure 3). The analytical results from PC1 to PC5 are presented in Table S10 of the Supplementary Material. The result shows that all elements can be characterized by three associations: (i) association with organic matter such as U, V, Zn, and Ni; (ii) association with carbonate (e.g., Ca) and rare earth elements (REEs); and (iii) association with aluminosilicates (e.g., Al, Ti, and Zr). We identify two groups based on the three associations: Group 1 comprises the LQS samples

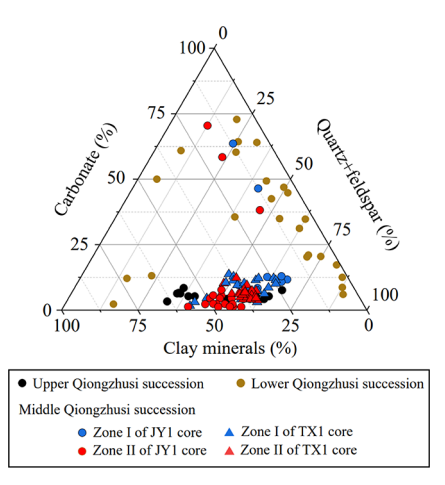


Figure 2. Ternary diagrams of clay minerals, quartz and feldspar, and carbonate in the Qiongzhusi succession.

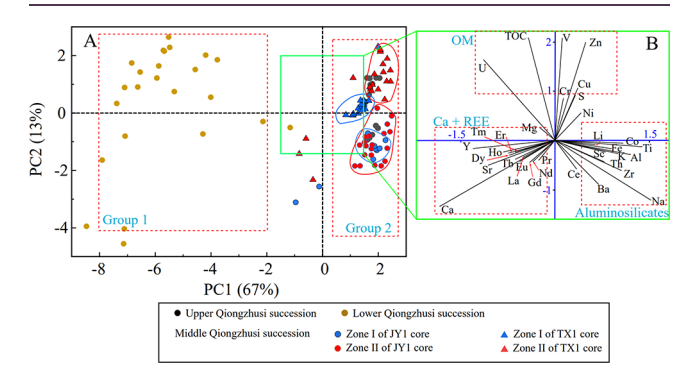


Figure 3. Biplot of scores and loading from principal component analysis (PCA) of elements and TOC of the TX1 and JY1 cores. The first principal component (PC1) accounts for 67%, and the PC2 is 13%. The top-five PC results are present in the Supplemental Material.

characterized by elements associated with organic matter, carbonate, and REEs. Group 2 encompasses elements affiliated with organic matter and aluminosilicates (the MQS–UQS samples). In addition, this model shows that elements associated with organic matter can distinguish samples deposited in the southern and northern parts of the MQS (Figure 3).

4.2.2. Uranium and Vanadium Associations with TOC. Because U and V concentrations are relatively low in our samples, it is important to remove the variation related to the mineral matrix and clastic lithophilic fractions before using U and V to identify redox conditions. Equation 1 used is as follows:

$$\Delta X = X_{\text{tot}} - \text{Al}_{\text{sample}} \times (X_{\text{PAAS}}/\text{Al}_{\text{PAAS}})$$
(1)

where X_{tot} is the total X concentration of the sample, ppm; Al_{sample} is the total Al content of the sample, %; X_{PAAS} is the X concentration of the PAAS, ppm; Al_{PAAS} is the Al content of the PAAS, %; and ΔX is the remaining X concentration after removing detrital influences.

Figure 4A shows that ΔV and TOC are significantly correlated in the LQS (R = 0.75; P < 0.05) and in the UQS (R = 0.87; P < 0.05), and Figure 4B shows that ΔU and TOC are significantly correlated (R = 0.74 for the LQS and R = 0.98 for the UQS; P < 0.05, respectively). In the MQS, TOC is

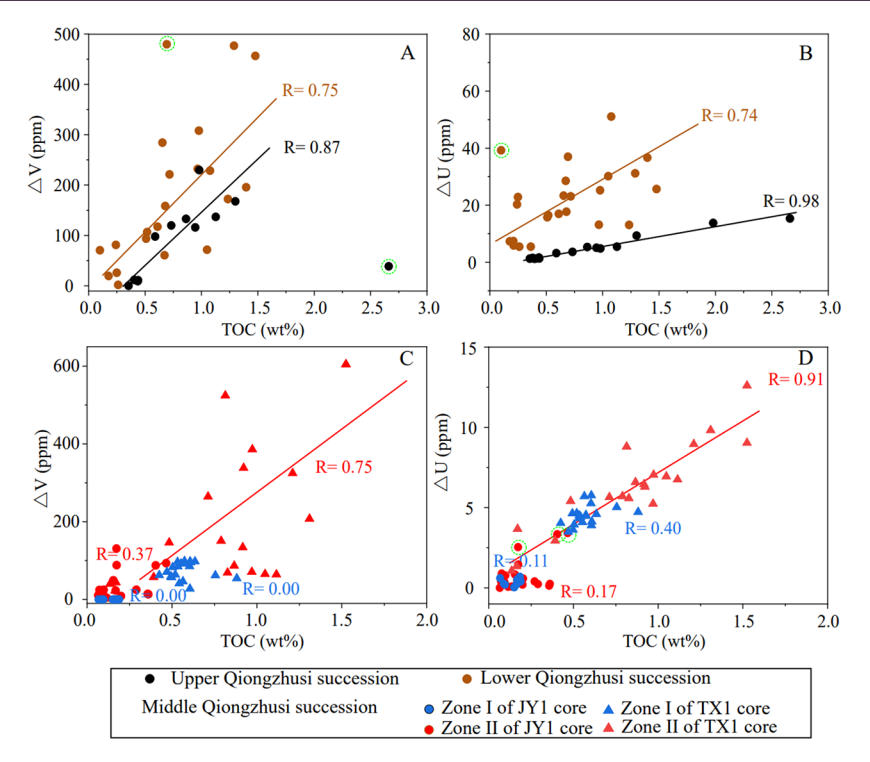


Figure 4. Crossplots of (A) the remaining V content after removing estimated detrital V component (ΔV) versus total organic matter (TOC) in the LQS and UQS, (B) the remaining U content after removing estimated detrital U component (ΔU) versus TOC in the LQS and UQS. (C) ΔV versus TOC in the MQS, and (D) ΔU versus TOC in the MQS.

correlated to ΔV (R = 0.75) and ΔU (R = 0.91) in only zone II of the TX1 core (Figure 4C,D).

4.2.3. Rare Earth Elements and Yttrium. The median value of REEs and Y in each succession of each core normalized by the PAAS²⁷ is shown in Figure 5 and Figure S3. The median

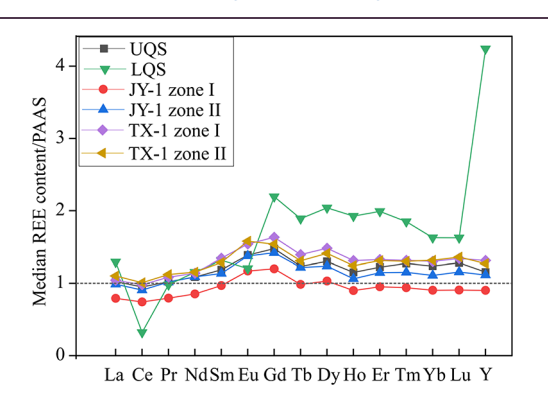


Figure 5. Distribution of rare earth elements (REEs) normalized to the Post Archean Australian Shale (PAAS) value (Taylor and McLennan, 1985). The median value of each REEs in each succession is used. The REE concentrations of each sample are shown in Figure S1 of the Supplemental Material.

REEs and Y values in the LQS have pronounced negative Ce and Eu anomalies, positive La and Y anomalies, and heavy REE (HREE) enrichments. The REEs and Y in the MQS–UQS show the same pattern with weak middle REE (MREE) enrichments. The MQS in the TX1 core is slightly enriched in REEs compared to the JY1 core. In this study, the Ce anomaly is defined as $Ce/Ce^* = 3Ce_N/(2La_N + Nd_N)$, the Pr anomaly is $Pr/Pr^* = 2Pr_N/(Ce_N + Nd_N)$, and the Eu anomaly is Eu/Eu* = $Eu_N/(Sm_N \times Gd_N)^{0.5}$ (N means that the element was normalized to the PAAS value) following Shields and Stille. ²⁸

5. DISCUSSION

5.1. Paleoredox Condition. *5.1.1. Redox Metal–TOC Relationship.* Under reducing conditions, U and V are generally correlated to TOC. Figure 4A–D show that ΔV and ΔU are significantly correlated to TOC in the LQS and UQS of JY1 core, as well as MQS zone II of the TX1 core. Those correlations indicate that the samples in the LQS and UQS, as well as in MQS zone II of the TX1 core, were deposited under reducing conditions. In the MQS, there are no relationships between TOC and ΔV (ΔU) in samples from the JY1 core and TX1 zone I. Those insignificant correlations suggest oxic to dysoxic conditions, from which limited amounts of U and V were reduced and hosted by organic matter (Figure 4C,D).

5.1.2. Mo–U Covariation. The Mo–U covariation is widely used to identify redox conditions.³² Under suboxic conditions of normal water settings, the enrichment of U generally exceeds that of Mo because U accumulation starts at the Fe(II)–Fe(III) redox boundary before Mo accumulation. As redox conditions become more reducing than suboxia, the Mo accumulation will exceed U. The Mo–U covariation is used to examine the redox condition of the JY1 core. Figure 6 shows that in the MQS, the samples were mainly deposited under oxic to suboxic conditions and Fe/Mn oxyhydroxides likely shuttled Mo and U. In contrast to the MQS, the samples in the UQS and LQS were deposited under more reducing conditions (suboxia–anoxia).

5.1.3. Redox Response of the REEs. The Ce anomaly can be used as a redox-sensitive tracer.³³ Under oxic conditions, the insoluble Ce(+III) is oxidized to soluble Ce(+IV), which could result in Ce depletion. The Ce anomaly is generally influenced by the La anomaly.²⁸ Figure 7A shows that the MQS-UQS samples are mainly located in Field IIa, whereas the LQS samples are mostly in Field IIIb, suggesting that the weakly

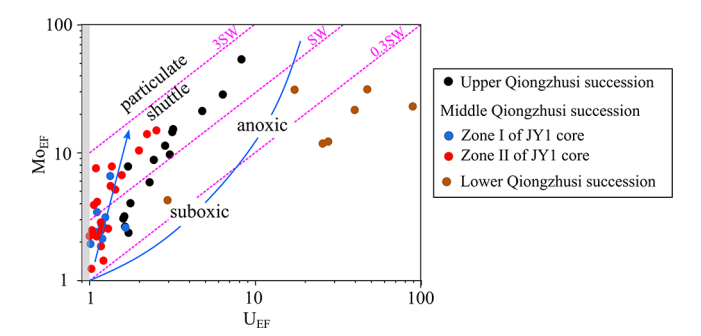


Figure 6. Enrichment factors of U (U_{EF}) versus Mo (Mo_{EF}) in the JY1 core. Modified from Algeo and Tribovillard.³²

negative Ce anomaly is influenced by positive La anomaly in the MQS-UQS, but the Ce anomaly seems to be realistic in the LOS.

Except for the influence of La anomaly, the negative Ce anomaly in the LQS can result from the following mechanisms: (i) organic matter, $^{34-36}$ (ii) diagenesis, 28 (iii) redox conditions, 37 (iv) detrital influx, 38 and (v) seawater. 39 Figure 7B shows that the Ce/Ce* ratio is not correlated to TOC, suggesting that the changes in organic matter have a limited influence on Ce anomaly. There are also insignificant correlations in Ce/Ce*–REE (Figure 7C) and Ce/Ce*–Dy_N/Sm_N (Figure 7D). We thus exclude the diagenetic effect. Figure 7E shows that the Ce/Ce* ratio is weakly correlated to Al (R=0.62), indicating that the detrital influx may be associated with negative Ce anomalies.

In addition, previous studies suggested that negative Ce and Eu anomalies and slight HREE enrichments in carbonate rocks reflect redistributions of REEs during dolomitization or the REE signature of the seawater from which they precipitated. ^{39–41} This specific pattern (negative Ce and Eu anomalies and HREEs enrichment) is also observed in the LQS samples (Figure 5). As stated above, the diagenetic process has a limited effect on Ce anomalies. We thus consider that the specific pattern is significantly attributed to the REE

signature in seawater. Sholkovitz et al.³⁹ investigated the REE pattern in the water column of the Sargasso Sea. Their results showed that the seawater has negative Ce and Eu anomalies with an overall HREEs-enriched composition from Gd to Lu. Therefore, we consider that the specific pattern (negative Ce and Eu anomalies and HREEs enrichment) in the LQS is most likely attributed to the REE signature of the seawater at the depositional time. By analogy with the Sargasso Sea, the redox condition is considered to be suboxic in the LQS.

5.2. Water Salinity and Restriction. Wei and Algeo⁴² suggested that Sr/Ba and S/TOC ratios can be used to investigate the paleowater salinity. The Sr/Ba ratio cannot be used but only after removing the carbonate-hosted Sr content that can be examined through the CaO-Sr/Ba relationship. With this pretreatment, a Sr/Ba ratio < 0.2 indicates freshwater, 1 > Sr/Ba > 0.2 suggests brackish water, and >0.5 shows marine water. When the TOC is above 0.5 wt %, the S/TOC ratio can be used to investigate the water salinity. In general, the S/TOC ratio is above 0.1 in brackish-marine water and is below 0.1 in freshwater. Figure S4A,B shows that the Sr/Ba ratio is not influenced by carbonate in the MQS-UQS. Therefore, the Sr/Ba ratio is used to examine the water salinity during the MQS and UQS. Figure 8A demonstrates that the MQS samples were deposited in brackish water and the UQS samples were deposited in fresh to slightly brackish water. In addition, Figure 8B indicates that the Qiongzhusi samples were deposited in a brackish-marine water setting. Given that the S/TOC ratio has relatively higher accuracy, we suggest that the MQS-UQS samples were deposited in a brackish-marine water setting.

The $Co_{EF} \times Mn_{EF}$ value can be indicative of water circulation and hydrographic restriction in modern and ancient marine systems. The upwelling of ocean water is characterized by low Co and Mn contents due to their depletion, whereas the restricted water mass is enriched in Co and Mn because of the terrestrial input. When the $Co_{EF} \times Mn_{EF}$ value is below 0.5, it is suggestive of an upwelling system, and when it is above 2, it indicates a restricted water setting. The $Co_{EF} \times Mn_{EF}$ values are between 0.5 and 2, which shows that the water circulation

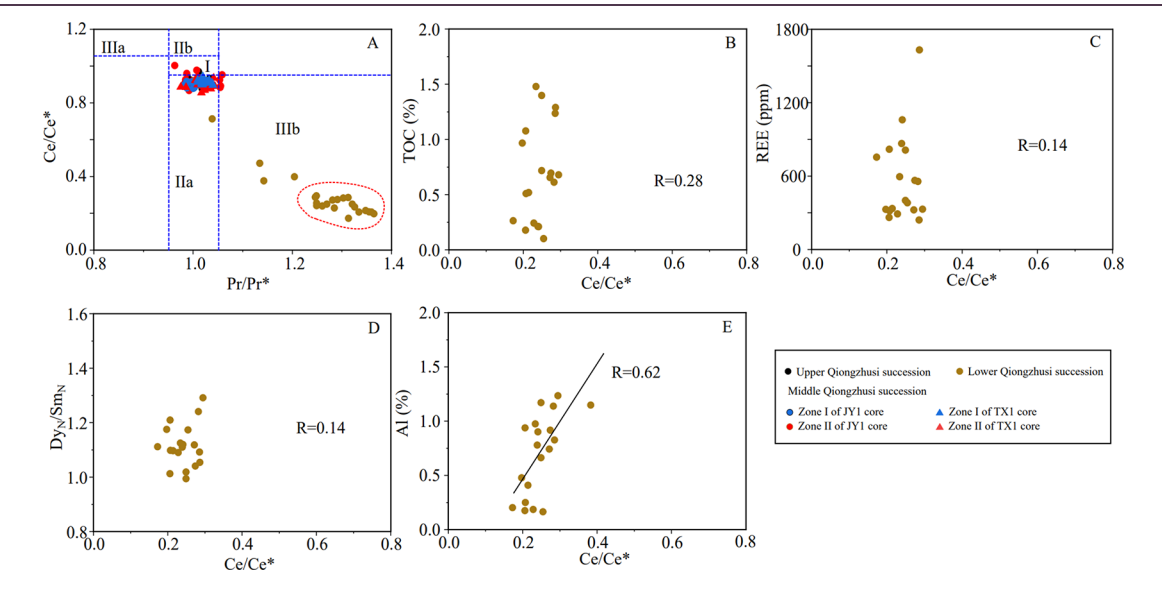


Figure 7. Plots of (A) Pr/Pr^* versus Ce/Ce^* , (B) Ce/Ce^* versus TOC, (C) Ce/Ce^* versus REE, (D) Ce/Ce^* versus Dy_N/Sm_N , and (E) Ce/Ce^* versus Al. In panel A: Field I, no anomaly; Field IIa, positive La anomaly causes apparent negative Ce anomaly; Field IIIb, negative La anomaly causes apparent positive Ce anomaly; Field IIIa, real positive Ce anomaly; and Field IIIb, real negative Ce anomaly (Shields and Stille²⁸).

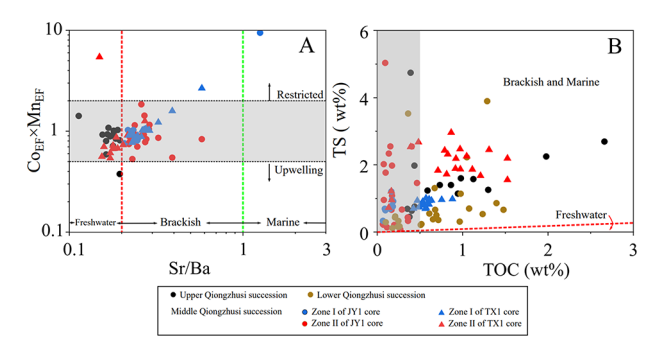


Figure 8. Plots of (A) Sr/Ba versus Co \times Mn and (B) TOC versus TS. The boundary for water circulation can refer to Sweere et al. and for water salinity is suggested in Wei and Algeo. In panel D, the vertical gray area represents invalid samples for identifying the paleowater salinity. Place of the paleowater salinity.

changed to the normal water circulation in the MQS-UQS (Figure 8C).

5.3. Paleoclimate and Detrital Influx. The paleoclimate can influence the intensity of detrital flux by affecting the terrestrial erosion rate. ⁴³ Proxies, such as C_{value} and Sr/Cu, can be used to indicate the paleoclimate. ⁸ The C_{value} is defined as

 C_{value} (wt %/wt %) = (Fe + Mn + Cr + Ni + V + Co)/(Ca + Mg + Sr. + Ba + K + Na). Because Fe, Mn, Cr, Ni, V, and Co are enriched in humid conditions and Ca, Mg, Sr, Ba, and K tend to precipitate under arid conditions, the increase in C_{value} indicates that the climate became more humid, and its decrease suggests more arid conditions. In addition, since humid conditions have high Cu content and arid conditions are enriched in Sr, the Sr/Cu ratio is also used to recognize humid-arid conditions. 44 Given that the C_{value} is not an effective proxy in carbonates and Sr is affected by carbonates in the LQS, the two proxies are only used to identify the MQS and UQS climates. Figure 9A shows that in the MQS, the northern part has higher C_{value} content and lower Sr/Cu ratios than the southern part. This indicates that the northern Sichuan Basin had more humid conditions. In the UQS, the samples with relatively high C_{value} contents (0.5–0.6) and low Sr/Cu ratio (1-3) have high TOC contents (average: 1.24%, n= 7), whereas the samples with low C_{value} content (0.3–0.5) and high Sr/Cu ratio (3-4) have low TOC contents (average: 0.4 wt %, n = 6). Those relationships suggest that the climate could have affected organic matter contents in the Sichuan

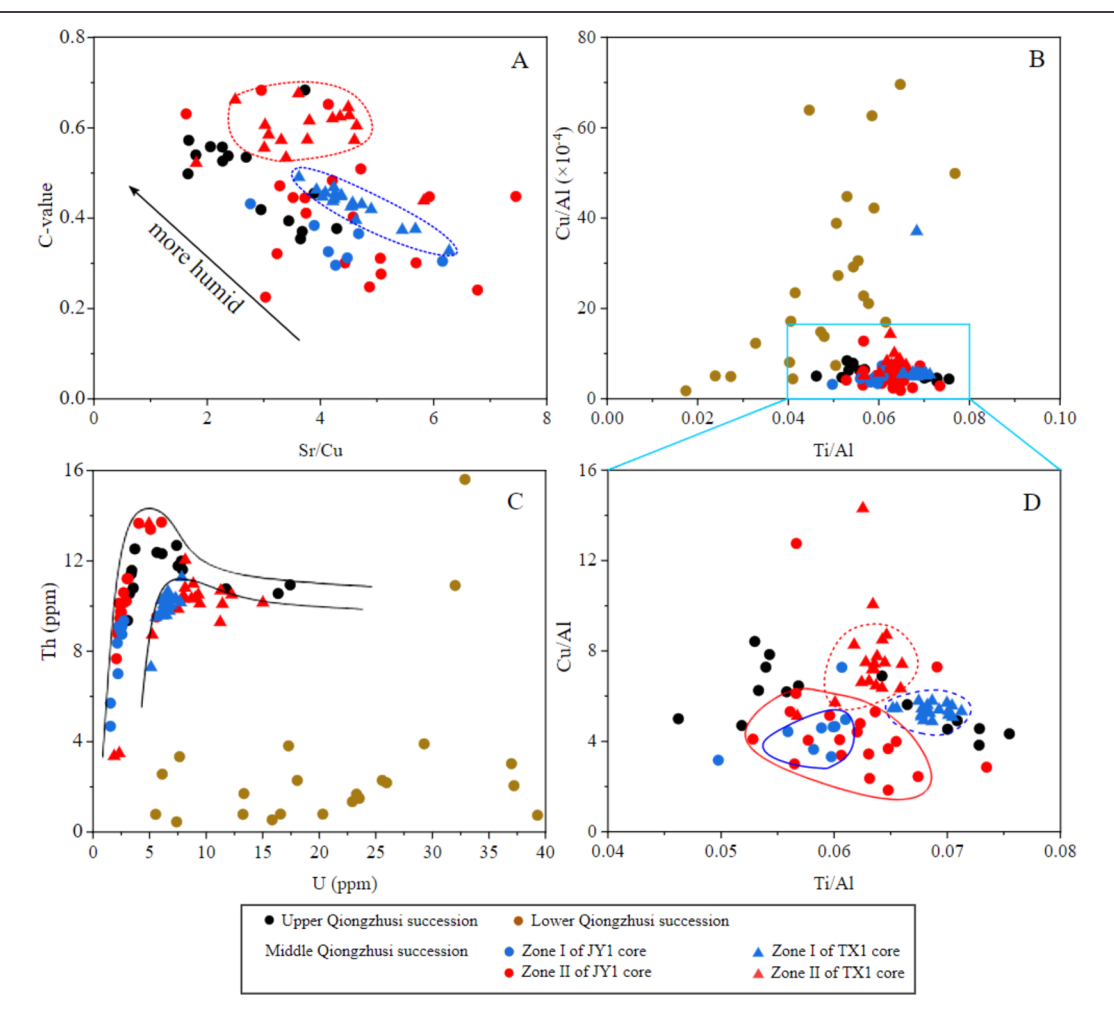


Figure 9. Plots of (A) Sr/Cu versus C_{value} (B) Ti/Al versus Cu/Al, (C) U versus Th, and (D) Ti/Al versus Cu/Al in the MQS-UQS. Panel D is an expansion of a part of panel B. In panel A, the blue-dashed line comprises all samples of zone I of the TX1 core whereas the red-dashed one represents the main range for the samples in zone II of the TX1 core. In panel C, the two curves indicate the relative changes in/between the JY1 and TX1 cores. In panel D, the curved lines are used to outline the main range of the samples in each succession of each core (the red-dashed line for the TX1-zone II, blue-dashed line for the TX1-zone II, and blue line circle for the JY1-zone I).

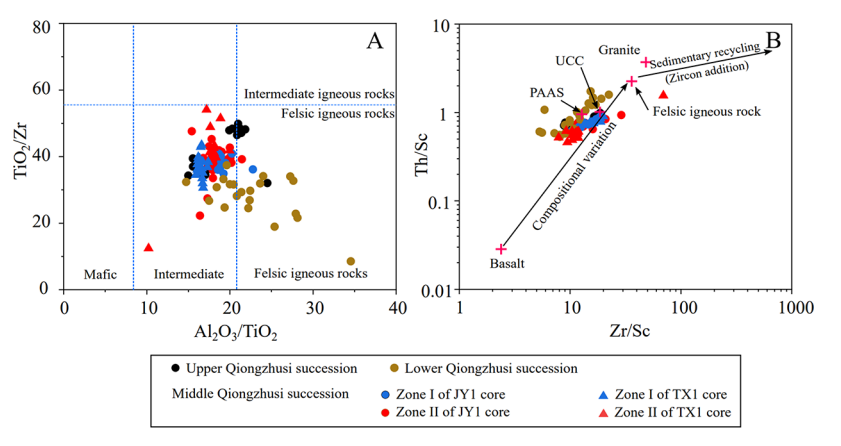


Figure 10. Plots of (A) Al₂O₃/TiO₂ versus TiO₂/Zr (Hayashi et al.⁵⁸) and (B) Zr/Sc versus Th/Sc. Modified from McLennan et al.⁵³

The intensity of detrital influx could be characterized by the Ti/Al ratio because Ti is commonly hosted by clay minerals and heavy minerals. The increase in the Ti/Al ratio indicates an elevated proportion of large grains (i.e., zircon) and increased terrestrial detrital influx. Figure 9B shows that the Ti/Al ratios are between 0.04 and 0.06 in the LQS, suggesting a low intensity of detrital influx. In the MQS, the low part (zone II) had a lower detrital input than the upper part (zone I; Figure 9D). In contrast to the southern part of the Sichuan Basin, the MQS in the northern basin had a relatively higher detrital influx input (Figure 9D). In the UQS, the samples with high TOC content have low Ti/Al ratios (<0.06), suggesting that the low intensity of detrital input was coincident with high organic matter burial (Figure 9D).

5.4. Primary Productivity and Sedimentation Rate. Copper (Cu) is an important nutrient for the biota as it can be incorporated into organic complexes and form essential metalloenzymes. 46 The commonly observed correlation between Cu abundance and the intensity of plankton productivity in modern and ancient environments made it possible to assess the paleoproductivity. 47-49 Therefore, it can be used to indicate primary productivity through being normalized to Al for the removal of the influence of terrestrial materials. 47,50 The Cu/Al ratios mainly exceed 10 \times 10^{-4} in the LQS and are between 2×10^{-4} and 10×10^{-4} in the MQS-UQS, suggesting a higher primary productivity in the LQS (Figure 11B,D). In the MQS, the Cu/Al ratios in the north $(5-9 \times 10^{-4})$ are relatively higher than in the south (2- 6×10^{-4}), indicating that the northern basin had a higher productivity. In the UQS, the samples with high TOC content had higher primary productivity $(6-8 \times 10^{-4})$, whereas the samples with low TOC content had lower productivity $(4-6 \times$ 10⁻⁴) (Figure 9). This seems to indicate that the variation in primary productivity could have influenced organic matter content.

Thorium (Th) is relatively non-leachable in sediments during the weathering and transport processes, 51,52 whereas U content is easily influenced during the depositional process. Therefore, the elevated Th/U ratio is used to indicate an elevated sedimentation rate. In the MQS, the distinct Th increase is coincident with the absence of U enrichment in the JY1 core (Figure 9C), which suggests that the high sedimentation rate was attributed to high rainfall and detrital input. In contrast to the JY1 core, the Th/U ratio in the TX1 core is lower, indicating a lower sedimentation rate (Figure 9C). The LQS samples have high U (5–40) and low Th

(mainly <4), which could be attributed to allochthonous U supplements and low sedimentation rates.

5.5. Provenance and Tectonic Setting. Rock provenance can affect the elemental composition in sedimentary rocks^{54,55} and the ecosystem by adjusting the nutrient input.⁵⁶ For example, felsic igneous rocks can result in a nutrient-poor condition, whereas mafic rocks can lead to a nutrient-rich condition. 57 The conservative elements and their major oxides (the Al₂O₃/TiO₂ ratio) can be used to decipher rock provenance.^{6,8} In general, Al₂O₃/TiO₂ < 8 indicates mafic igneous rocks, >8 and <21 suggests intermediate igneous rocks, and >21 indicates felsic igneous rocks. The TiO₂/Zr ratio can also indicate mafic (>194), intermediate (54-194), and felsic igneous rocks (<54).⁵⁸ The Al₂O₃/TiO₂ ratio ranges between 15 and 21 in the MQS-UQS, which suggests that the rock provenance was intermediate igneous rocks, whereas the Al₂O₃/TiO₂ ratio varies between 15 and 20 in the LQS, indicating that the rock source was intermediate—felsic igneous rocks (Figure 10A). The TiO₂/Zr ratio in the Qiongzhusi is below 54, representing that the rock provenance was felsic igneous rocks (Figure 10A). Figure 10B shows that the rock provenance was between basalt and felsic igneous rocks and closer to felsic igneous rocks.⁵³ In addition, the stable elemental assemblages indicate no significant sedimentary recycling. Therefore, we conclude that the rock provenance was intermediate-felsic igneous rocks in the Qiongzhusi.

Identifying tectonic settings is significant as it can influence the elemental transport and ultimate distribution in sedimentary archives. ^{59,60} For example, organic matter-associated metals within a rifted basin tend to accumulate in the gentle-slope side because they have relatively favorable depositional conditions ⁶¹ that can support the formation of reducing conditions and facilitate redox metal sequestrations. ^{62,63} Previous studies suggested that the stable elemental associations can be used to infer tectonic settings, owing to their relative stabilities during the transport process. ^{64–66} The ternary diagrams of Co–Th–Zr/10 and Sc–Th–Zr/10 can identify four tectonic settings: oceanic island arc, continental island arc, active continental margin, and passive continental margin. ⁶⁷ Figure 11 shows that the depositional setting in the Qiongzhusi Formation was a continental island arc.

5.6. Controls on Organic Matter Accumulation. Primary organic matter productivity and preservation are influenced by atmospheric, tectonic, oceanic, and biological factors. ^{68–71} In the Qiongzhusi Formation of Sichuan Basin, the rock provenance was intermediate to felsic igneous rocks

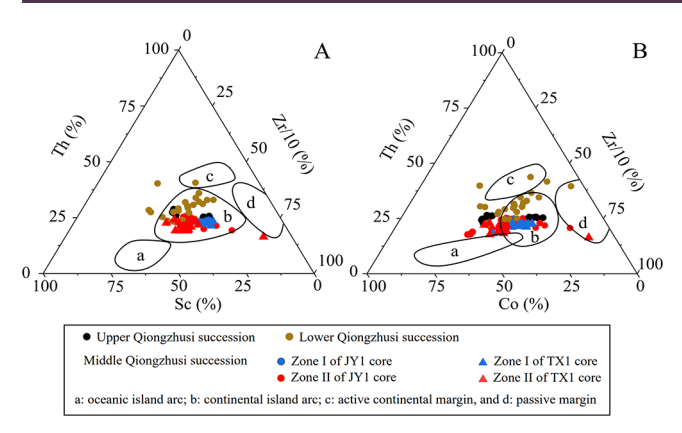


Figure 11. Ternary diagrams of (A) Co–Th–Zr/10 and (B) Sc–Th–Zr/10. Modified from Bhatia and Crook. 67

that may contribute to a nutrient-poor condition.⁵⁷ The tectonic setting was likely to be a continental island arc, which suggests a relatively variable depositional condition that may have impeded the development of the ecosystem. Because the Mianyang—Changning sag had a relatively gentle western slope and a relatively steep eastern slope, it is inferred that excellent organic matter accumulation areas could have occurred closer to the western slope. In addition, during the Qiongzhusi Formation, the samples were deposited into the brackishmarine water, indicating the paleosalinity is not a crucial factor for interpreting differential organic matter contents in the MQS–UQS (Figure 12).

In contrast to the southern (the JY1 core) part of the Sichuan Basin, the northern part (the TX1 core) has a higher TOC content, which coincides with higher organic matter productivity, more humid climate, lower sedimentation rate, and lower detrital input. Those proxies indicate a more suitable condition for biological development. In addition, the reducing depositional conditions could have partially contributed to organic matter preservation (Figure 12).

Compared to the MQS, the LQS and UQS had higher organic matter productivity and more humid conditions, and the samples in the two successions were deposited into more reducing conditions with lower sedimentation rates and detrital inputs. These depositional conditions could have contributed to better organic matter productivity and preservation. Compared to the MQS and UQS, the LQS had a restricted water setting and was not influenced by ocean water upwelling identified in the southern Yangtze Platform. This situation may have partially resulted in a relatively stable

environment for the ecosystem and further interpreted relatively high organic matter preservation in the LQS (Figure 12).

6. CONCLUSIONS

This paper investigated the spatial and temporal variations of elements and TOC as related to the lower Cambrian depositional environment of the Sichuan Basin. We conclude that:

- (1) The Qiongzhusi source rock demonstrates three distinct elemental groups: (i) REEs and carbonate-associated elements (e.g., Ca) for characterizing the lower Qiongzhusi (LQS) samples, (ii) aluminosilicate elements (e.g., Al and Ti) for identifying the middle and upper Qiongzhusi samples (MQS and UQS), and (iii) organic matter-associated metals (e.g., V and U) for differentiating the southern and the northern samples in the MQS.
- (2) The elemental composition suggests that the tectonic setting was a continental island arc and the rock provenance was intermediate-felsic igneous rocks. The Sr/Ba and S/TOC proxies indicate that the Qiongzhusi samples were deposited into a brackish-marine water setting.
- (3) In contrast to the MQS, the $\Delta V/\Delta U$ -TOC relationship and the Mo_{EF}-U_{EF} covariation suggest more reducing conditions, the Ti/Al and Th/U ratios indicate relatively lower detrital inputs and sedimentation rates, and the Cu/Al ratio implies higher primary productivity in the LQS and UQS. Therefore, we suggest that the LQS and UQS had better depositional conditions for organic matter productivity and preservation.
- (4) Compared to the southern Sichuan Basin, the northern part (the TX1 core) had a more humid condition interpreted by higher C_{value} contents and lower Sr/Cu ratios, more reducing conditions (the $\Delta V(\Delta U)$ –TOC correlations), a higher nutrient supply (high Cu/Al ratios), and a lower sedimentation rate (low Th/U ratios).

ASSOCIATED CONTENT

Supporting Information

The Supporting Information is available free of charge at https://pubs.acs.org/doi/10.1021/acsearthspace-chem.2c00224.

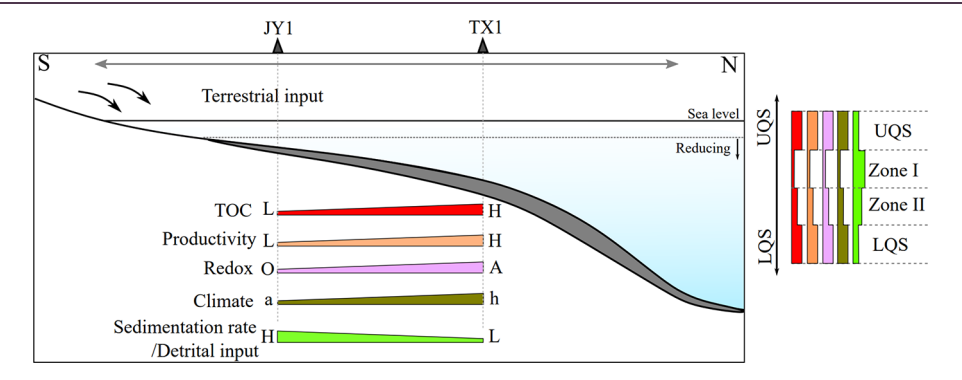


Figure 12. Schematic model of proxies for identification of depositional conditions. L is low, H is high, O is oxic, A is anoxic, a is arid, and h is humid. The width of each symbol can represent the variation of each proxy.

Vertical variation within the two cores; (Figures S1 and S2) Geochemical profiles of the JY1 core and TX1 core; (Figure S3) Distribution of rare earth elements (REE) and yttrium (Y) normalized to the Post Archean Australian Shale (PAAS) value in the Qiongzhusi Formation; (Figure S4) plots of CaO versus Sr/Ba and its regional expansion; (Tables S1–S10) analytical datasets of JY1 and TX1 cores (PDF)

AUTHOR INFORMATION

Corresponding Authors

Leibo Bian — State Key Laboratory of Shale Oil and Gas Enrichment and Effective Development, Wuxi, Jiangsu 214126, China; Lithospheric Organic Carbon (LOC) Group, Department of Geoscience, Aarhus University, Aarhus 8000C, Denmark; orcid.org/0000-0002-0093-2671; Email: leibo@geo.au.dk

Hamed Sanei – Lithospheric Organic Carbon (LOC) Group, Department of Geoscience, Aarhus University, Aarhus 8000C, Denmark; Email: sanei@geo.au.dk

Authors

Niels H. Schovsbo — Department of Reservoir Geology, Geological Survey of Denmark and Greenland, Copenhagen DK1350, Denmark; © orcid.org/0000-0003-4723-0586

Anthony Chappaz – STARLAB, Department of Earth and Atmospheric Sciences, Central Michigan University, Mount Pleasant, Michigan 48859, United States; orcid.org/0000-0001-8713-8456

Arka Rudra – Lithospheric Organic Carbon (LOC) Group, Department of Geoscience, Aarhus University, Aarhus 8000C, Denmark

Jin Xu – State Key Laboratory of Shale Oil and Gas Enrichment and Effective Development, Wuxi, Jiangsu 214126, China

Qingyong Luo — State Key Laboratory of Petroleum Resources and Prospecting, China University of Petroleum, Beijing 102249, China; orcid.org/0000-0002-1176-5709

Complete contact information is available at: https://pubs.acs.org/10.1021/acsearthspacechem.2c00224

Author Contributions

L.B. was in charge of conceptualization, investigation, methodology, software, sampling, validation, formal analysis, data curation, writing the original draft, reviewing and editing the final manuscript, and data visualization. N.H.S. was in charge of supervision, conceptualization, methodology, validation, formal analysis, data curation, and reviewing and editing the final manuscript. A.C. was in charge of supervision, validation, formal analysis, and reviewing and editing the final manuscript. H.S. was in charge of supervision, conceptualization, methodology, validation, formal analysis, reviewing and editing the final manuscript, and funding acquisition. A.R. and others were in charge of validation and formal analysis.

Notes

The authors declare no competing financial interest.

ACKNOWLEDGMENTS

All authors acknowledge Prof. James C. Hower and Dr. Stefan V. Lalonde for significant scientific advices. We thank support from the China University of Petroleum (Beijing) (H.S.), GeoCenter Denmark Project 2017-3 (N.S.), CSC scholarship

and AAPG Grant-in-Aids (L.B.), NSF-EAR grant 2051199 (A.C.), and grant no. SKLOG202115.

REFERENCES

- (1) Lu, Y.; Jiang, S.; Lu, Y.; et al. Productivity or preservation? The factors controlling the organic matter accumulation in the late Katian through Hirnantian Wufeng organic-rich shale, South China. *Mar. Pet. Geol.* **2019**, *109*, 22–35.
- (2) Wang, X.; Zhu, Y.; Lash, G. G.; Wang, Y. Multi-proxy analysis of organic matter accumulation in the Upper Ordovician—Lower Silurian black shale on the Upper Yangtze Platform, south China. *Mar. Pet. Geol.* **2019**, *103*, 473—484.
- (3) Sperling, E. A.; Melchin, M. J.; Fraser, T.; Stockey, R. G.; Farrell, U. C.; Bhajan, L.; Brunoir, T. N.; Cole, D. B.; Gill, B. C.; Lenz, A.; Loydell, D. K.; Malinowski, J.; Miller, A. J.; Plaza-Torres, S.; Bock, B.; Rooney, A. D.; Tecklenburg, S. A.; Vogel, J. M.; Planavsky, N. J.; Strauss, J. V. A long-term record of early to mid-Paleozoic marine redox change. *Sci. Adv.* 2021, 7, eabf4382.
- (4) Tan, J.; Wang, Z.; Wang, W.; et al. Depositional environment and fvhydrothermal controls on organic matter enrichment in the lower Cambrian Niutitang shale, southern China. *AAPG Bull.* **2021**, *105*, 1329–1356.
- (5) Sweere, T.; van den Boorn, S.; Dickson, A. J.; Reichart, G. J. Definition of new trace-metal proxies for the controls on organic matter enrichment in marine sediments based on Mn, Co, Mo and Cd concentrations. *Chem. Geol.* **2016**, *441*, 235–245.
- (6) Tao, S.; Xu, Y.; Tang, D.; et al. Geochemistry of the Shitoumei oil shale in the Santanghu Basin, Northwest China: Implications for paleoclimate conditions, weathering, provenance and tectonic setting. *Int. J. Coal Geol.* **2017**, *184*, 42–56.
- (7) Gill, B. C.; Dahl, T. W.; Hammarlund, E. U.; et al. Redox dynamics of later Cambrian oceans. *Palaeogeogr. Palaeoclimatol. Palaeoecol.* **2021**, 581, 110623.
- (8) Li, Q.; Wu, S.; Xia, D.; et al. Major and trace element geochemistry of the lacustrine organic-rich shales from the Upper Triassic Chang 7 Member in the southwestern Ordos Basin, China: Implications for paleoenvironment and organic matter accumulation. *Mar. Pet. Geol.* **2020**, *111*, 852–867.
- (9) Zou, C.; Zhu, R.; Chen, Z. Q.; et al. Organic matter-rich shales of China. Earth Sci. Rev. 2019, 189, 51–78.
- (10) Gao, P.; He, Z.; Lash, G. G.; et al. Controls on silica enrichment of Lower Cambrian organic-rich shale deposits. *Mar. Pet. Geol.* **2021**, *130*, 105126.
- (11) Gao, P.; Li, S.; Lash, G. G.; Yan, D.; Zhou, Q.; Xiao, X. Stratigraphic framework, redox history, and organic matter accumulation of an Early Cambrian intraplatfrom basin on the Yangtze Platform, South China. *Mar. Pet. Geol.* **2021**, *130*, 105095.
- (12) Qiu, N.; Liu, W.; Fu, X.; et al. Maturity evolution of Lower Cambrian Qiongzhusi Formation shale of the Sichuan Basin. *Mar. Pet. Geol.* **2021**, *128*, 105061.
- (13) Tang, Y.; Chen, Z.; Simoneit, B. R.; Wang, T. G.; Ni, Z.; Li, M.; Wen, L.; Yang, C. Recognition of in situ oil cracking in the precambrian—lower Cambrian petroleum systems of Sichuan basin, southwestern China. *Mar. Pet. Geol.* **2021**, *126*, 104942.
- (14) Gao, P.; Liu, G.; Jia, C.; et al. Redox variations and organic matter accumulation on the Yangtze carbonate platform during Late Ediacaran—Early Cambrian: constraints from petrology and geochemistry. *Palaeogeogr. Palaeoclimatol. Palaeoecol.* **2016**, 450, 91–110.
- (15) Zhang, P.; Liu, G.; Cai, C.; Li, M.; Chen, R.; Gao, P.; Xu, C.; Wan, W.; Zhang, Y.; Jiang, M. Alteration of solid bitumen by hydrothermal heating and thermochemical sulfate reduction in the Ediacaran and Cambrian dolomite reservoirs in the Central Sichuan Basin, SW China. *Precambrian Res.* **2019**, *321*, 277–302.
- (16) Liu, S.; Deng, B.; Jansa, L.; Zhong, Y.; Sun, W.; Song, J.; Wang, G.; Wu, J.; Li, Z.; Tian, Y. The early Cambrian mianyang-changning intracratonic sag and its control on petroleum accumulation in the Sichuan Basin, China. *Geofluids.* **2017**, 1.
- (17) Li, Z. X.; Bogdanova, S.; Collins, A. S.; Davidson, A.; de Waele, B.; Ernst, R. E.; Fitzsimons, I. C. W.; Fuck, R. A.; Gladkochub, D. P.;

- Jacobs, J.; Karlstrom, K. E.; Lu, S.; Natapov, L. M.; Pease, V.; Pisarevsky, S. A.; Thrane, K.; Vernikovsky, V. Assembly, configuration, and break-up history of Rodinia: a synthesis. *Precambrian Res.* **2008**, *160*, 179–210.
- (18) Feng, L.; Li, C.; Huang, J.; Chang, H.; Chu, X. A sulfate control on marine mid-depth euxinia on the early Cambrian (ca. 529–521 Ma) Yangtze platform, South China. *Precambrian Res.* **2014**, *246*, 123–133.
- (19) Chang, X.; Yao, S.; Song, D.; Liu, Y. Types, chemical and porosity characteristics of hydrocarbon-generating organisms of the lower Paleozoic, south China-Taking Longmaxi Formation and Qiongzhusi Formation in Sichuan Basin as examples. *Mar. Pet. Geol.* 2020, 119, 104508.
- (20) Yang, B.; Steiner, M. Terreneuvian bio- and chemostratigraphy of the South Sichuan Region (South China). J. Geol. Soc. 2021, 178.
- (21) Liu, J.; Zhang, K. Y. Sedimentary facies characteristics of Maidiping-Qiongzhusi formation in Jingyan-Qianwei area. *Sci. Technol. Eng.* **2018**, *18*, 20–25 (In Chinese with English abstract).
- (22) Xia, G.; Ran, B.; Liu, S.; et al. Chacteristics of hydrocarbon source rocks of the Lower Cambrian Maidiping Formation in northern Miangyang-Changning intracratonic sag, Sichuan, China. *J. Chengdu Univ. Technol. (Sci. Technol. Ed.)* **2018**, *45*, 14–26. (In Chinese with English abstract)
- (23) Young, R. A. *The rietveld method*; International union of crystallography. 1993, 5, 1–38.
- (24) Valls, R. A. Why, and how, we should use compositional data analysis—A step-by-step guide for field geologists; Wikibooks: Toronto, 2008
- (25) Hammer, Ø. Past: Paleontological Statistics (version 3.25)-reference manual. Natural History Museum, University of Olso, 2019.
- (26) Bian, L.; Schovsbo, N. H.; Chappaz, A.; et al. Molybdenum-uranium-vanadium geochemistry in the lower Paleozoic Alum Shale of Scandinavia: Implications for vanadium exploration. *Int. J. Coal Geol.* **2021**, 239, 103730.
- (27) Taylor, S. R.; McLennan, S. M. The continental crust: its composition and evolution; Blackwell; Oxford, 1985.
- (28) Shields, G.; Stille, P. Diagenetic constraints on the use of cerium anomalies as palaeoseawater redox proxies: an isotopic and REE study of Cambrian phosphorites. *Chem. Geol.* **2001**, *175*, 29–48.
- (29) Bone, S. E.; Dynes, J. J.; Cliff, J.; Bargar, J. R. Uranium (IV) adsorption by natural organic matter in anoxic sediments. *Proc. Natl. Acad. Sci. U. S. A.* **2017**, *114*, 711–716.
- (30) Breit, G. N.; Wanty, R. B. Vanadium accumulation in carbonaceous rocks: a review of geochemical controls during deposition and diagenesis. *Chem. Geol.* **1991**, *91*, 83–97.
- (31) Algeo, T. J.; Maynard, J. B. Trace-element behavior and redox facies in core shales of Upper Pennsylvanian Kansas-type cyclothems. *Chem. Geol.* **2004**, 206, 289–318.
- (32) Algeo, T. J.; Tribovillard, N. Environmental analysis of paleoceanographic systems based on molybdenum-uranium covariation. *Chem. Geol.* **2009**, 268, 211–225.
- (33) German, C. R.; Elderfield, H. Application of the Ce anomaly as a paleoredox indicator: the ground rules. *Paleoceanography* **1990**, *5*, 823–833.
- (34) Tang, J.; Johannesson, K. H. Speciation of rare earth elements in natural terrestrial waters: assessing the role of dissolved organic matter from the modeling approach. *Geochim. Cosmochim. Acta* **2003**, 67, 2321–2339.
- (35) Tang, J.; Johannesson, K. H. Ligand extraction of rare earth elements from aquifer sediments: implications for rare earth element complexation with organic matter in natural waters. *Geochim. Cosmochim. Acta* **2010**, *74*, 6690–6705.
- (36) Gao, P.; Liu, G.; Wang, Z.; et al. Rare earth elements (REEs) geochemistry of Sinian—Cambrian reservoir solid bitumens in Sichuan Basin, SW China: potential application to petroleum exploration. *Geol. J.* **2017**, *52*, 298–316.
- (37) Elderfield, H.; Greaves, M. J. The rare earth elements in seawater. *Nature* **1982**, *296*, 214–219.

- (38) Auer, G.; Reuter, M.; Hauzenberger, C. A.; Piller, W. E. The impact of transport processes on rare earth element patterns in marine authigenic and biogenic phosphates. *Geochim. Cosmochim. Acta* **2017**, 203, 140–156.
- (39) Sholkovitz, E. R.; Landing, W. M.; Lewis, B. L. Ocean particle chemistry: the fractionation of rare earth elements between suspended particles and seawater. *Geochim. Cosmochim. Acta* **1994**, *58*, 1567–1579.
- (40) Qing, H.; Mountjoy, E. W. Rare earth element geochemistry of dolomites in the Middle Devonian Presqu'ile barrier, Western Canada Sedimentary Basin: implications for fluid-rock ratios during dolomitization. *Sedimentology* **1994**, *41*, 787–804.
- (41) Bellanca, A.; Masetti, D.; Neri, R. Rare earth elements in limestone/marlstone couplets from the Albian-Cenomanian Cismon section (Venetian region, northern Italy): assessing REE sensitivity to environmental changes. *Chem. Geol.* 1997, 141, 141–152.
- (42) Wei, W.; Algeo, T. J. Elemental proxies for paleosalinity analysis of ancient shales and mudrocks. *Geochim. Cosmochim. Acta* **2020**, 287, 341–366.
- (43) Tanaka, K.; Akagawa, F.; Yamamoto, K.; et al. Rare earth element geochemistry of Lake Baikal sediment: its implication for geochemical response to climate change during the Last Glacial/Interglacial transition. *Quat. Sci. Rev.* **2007**, *26*, 1362–1368.
- (44) Moradi, A. V.; Sari, A.; Akkaya, P. Geochemistry of the Miocene oil shale (Haneili Formation) in the Çankırı-Çorum Basin, Central Turkey: Implications for paleoclimate conditions, source—area weathering, provenance and tectonic setting. *Sediment. Geol.* **2016**, 341, 289–303.
- (45) Zhao, J.; Jin, Z.; Jin, Z.; Geng, Y.; Wen, X.; Yan, C. Applying sedimentary geochemical proxies for paleoenvironment interpretation of organic-rich shale deposition in the Sichuan Basin. *China. Int. J. Coal Geol.* **2016**, *163*, 52–71.
- (46) Osredkar, J.; Sustar, N. Copper and zinc, biological role and significance of copper/zinc imbalance. *J. Clinic Toxicol. S* **2011**, *s3*, 0495.
- (47) Tribovillard, N.; Algeo, T. J.; Lyons, T.; Riboulleau, A. Trace metals as paleoredox and paleoproductivity proxies: an update. *Chem. Geol.* **2006**, 232, 12–32.
- (48) Tribovillard, N. Re-assessing copper and nickel enrichments as paleo-productivity proxies. *BSGF-Earth Sci. Bull.* **2021**, 192, 54.
- (49) Li, Y.; Liu, W.; Liu, P.; et al. Paleoenvironment and Organic Matter Enrichment of the Middle Ordovician Marine Carbonates in the Ordos Basin of China: Evidence from Element Geochemistry. ACS Earth Space Chem. 2022, 6, 44–55.
- (50) Schoepfer, S. D.; Shen, J.; Wei, H.; et al. Total organic carbon, organic phosphorus, and biogenic barium fluxes as proxies for paleomarine productivity. *Earth Sci. Rev.* **2015**, *149*, 23–52.
- (51) Goodarzi, F.; Gentzis, T.; Sanei, H.; Pedersen, P. K. Elemental composition and organic petrology of a lower carboniferous-age freshwater oil shale in Nova Scotia, Canada. ACS Omega 2019, 4, 20773–20786.
- (52) Goodarzi, F.; Nina, N. G.; Malachowska, A. Elemental composition, environment of deposition of the Lower Carboniferous Emma Fiord Formation oil shale in Arctic Canada. *Int. J. Coal Geol.* **2021**, 103715.
- (53) McLennan, S. M.; Hemming, S.; McDaniel, D. K.; Hanson, G. N. Geochemical approaches to sedimentation, provenance, and tectonics. *Spec. Pap. Geol. Soc. Am.* **1993**, 284, 21–40.
- (54) Basu, A.; Bickford, M. E.; Deasy, R. Inferring tectonic provenance of siliciclastic rocks from their chemical compositions: A dissent. *Sediment. Geol.* **2016**, 336, 26–35.
- (55) Moyen, J. F.; Laurent, O. Archaean tectonic systems: A view from igneous rocks. *Lithos* **2018**, *302*, 99–125.
- (56) Aciego, S. M.; Riebe, C. S.; Hart, S. C.; et al. Dust outpaces bedrock in nutrient supply to montane forest ecosystems. *Nat. Commun.* **2017**, *8*, 1–10.
- (57) Large, R. R.; Mukherjee, I.; Zhukova, I.; et al. Role of uppermost crustal composition in the evolution of the Precambrian ocean—atmosphere system. *Earth Planet. Sci. Lett.* **2018**, 487, 44—53.

- (58) Hayashi, K. I.; Fujisawa, H.; Holland, H. D.; Ohmoto, H. Geochemistry of ~1.9 Ga sedimentary rocks from northeastern Labrador, Canada. *Geochim. Cosmochim. Acta* 1997, 61, 4115–4137.
- (59) McLennan, S. M.; Hemming, S. Samarium/neodymium elemental and isotopic systematics in sedimentary rocks. *Geochim. Cosmochim. Acta* **1992**, *56*, 887–898.
- (60) Hu, F.; Meng, Q.; Liu, Z. Mineralogy and element geochemistry of oil shales in the Lower Cretaceous Qingshankou Formation of the southern Songliao Basin, northeast China: implications of provenance, tectonic setting, and paleoenvironment. ACS Earth Space Chem. 2021, 5, 365–380.
- (61) Ding, X.; Liu, G.; Zha, M.; et al. Characteristics and origin of lacustrine source rocks in the Lower Cretaceous, Erlian Basin, northern China. *Mar. Pet. Geol.* **2015**, *66*, 939–955.
- (62) Chappaz, A.; Gobeil, C.; Tessier, A. Geochemical and anthropogenic enrichments of Mo in sediments from perennially oxic and seasonally anoxic lakes in Eastern Canada. *Geochim. Cosmochim. Acta* **2008**, 72, 170–184.
- (63) Bian, L.; Chappaz, A.; Schovsbo, N. H.; et al. High mercury enrichments in sediments from the Baltic continent across the late Cambrian: Controls and implications. *Chem. Geol.* **2022**, *599*, 120846.
- (64) Armstrong-Altrin, J. S.; Verma, S. P. Critical evaluation of six tectonic setting discrimination diagrams using geochemical data of Neogene sediments from known tectonic settings. *Sediment. Geol.* **2005**, *177*, 115–129.
- (65) Makeen, Y. M.; Abdullah, W. H.; Ayinla, H. A.; et al. Organic geochemical characteristics and depositional setting of Paleogene oil shale, mudstone and sandstone from onshore Penyu Basin, Chenor, Pahang, Malaysia. *Int. J. Coal Geol.* **2019**, 207, 52–72.
- (66) Qadrouh, A. N.; Alajmi, M. S.; Alotaibi, A. M.; Baioumy, H.; Almalki, M. A.; Alyousif, M. M.; Ahmed Salim, A. M.; Bin Rogaib, A. M. Mineralogical and geochemical imprints to determine the provenance, depositional environment, and tectonic setting of the Early Silurian source rock of the Qusaiba shale, Saudi Arabia. *Mar. Pet. Geol.* 2021, 130, 105131.
- (67) Bhatia, M. R.; Crook, K. A. W. Trace element characteristics of graywackes and tectonic setting discrimination of sedimentary basins. *Contrib. Mineral. Petrol.* **1986**, 92, 181–193.
- (68) Blattmann, T. M.; Liu, Z.; Zhang, Y.; et al. Mineralogical control on the fate of continentally derived organic matter in the ocean. *Science* **2019**, *366*, 742–745.
- (69) Kemp, D. B.; Baranyi, V.; Izumi, K.; Burgess, R. D. Organic matter variations and links to climate across the early Toarcian oceanic anoxic event (T-OAE) in Toyora area, southwest Japan. *Palaeogeogr. Palaeoclimatol. Palaeoecol.* **2019**, 530, 90–102.
- (70) Marín, D.; Helleren, S.; Escalona, A.; et al. The Middle Jurassic to lowermost Cretaceous in the SW Barents Sea: Interplay between tectonics, coarse-grained sediment supply and organic matter preservation. *Basin Res.* **2021**, 33, 1033–1055.
- (71) Owens, J. D.; Lyons, T. W.; Lowery, C. M. Quantifying the missing sink for global organic carbon burial during a Cretaceous oceanic anoxic event. *Earth Planet. Sci. Lett.* **2018**, 499, 83–94.

☐ Recommended by ACS

Controlling Factors and Formation Models of Organic Matter Accumulation for the Upper Permian Dalong Formation Black Shale in the Lower Yangtze Region, Sou...

Jianghui Ding, Chuxiong Li, et al.

JANUARY 27, 2021

ACS OMEGA

READ 🗹

Organic Matter Accumulation in the Youganwo Formation (Middle Eocene), Maoming Basin, South China: Constraints from Multiple Geochemical Proxies and Organic Petrology

Chuan Xu, Wentong He, et al.

MARCH 04, 2022

ACS EARTH AND SPACE CHEMISTRY

READ 🗹

Controls on Organic Matter Accumulation of the Triassic Yanchang Formation Lacustrine Shales in the Ordos Basin, North China

Xiaoliang Chen, Zhiguo Mao, et al.

OCTOBER 01, 2021

ACS OMEGA

READ 🗹

Mineralogy and Element Geochemistry of Oil Shales in the Lower Cretaceous Qingshankou Formation of the Southern Songliao Basin, Northeast China: Implications of Provena...

Fei Hu, Zhaojun Liu, et al.

FEBRUARY 08, 2021

ACS EARTH AND SPACE CHEMISTRY

READ 🗹

Get More Suggestions >